Odour encoding by temporal sequences of firing in oscillating neural assemblies

Michael Wehr & Gilles Laurent

California Institute of Technology, Biology Division, Pasadena, California 91125, USA

STIMULUS-EVOKED oscillatory synchronization of activity has been observed in many neural systems, including the cerebral cortex of mammals and the brain of insects[1–8]. The possible functions of such rhythmic synchronization in neural coding, however, remain largely speculative[9–13]. In the locust, odours evoke activity in dynamic (evolving) ensembles of transiently synchronized neurons[8,14,15]. We report here that the active neurons composing these ensembles change in a stimulus-specific manner and with a high degree of reliability on a cycle-by-cycle basis during an odour response. Hence, information about an odour is contained not only in the neural assembly active at each oscillation cycle, but also in the precise temporal sequence in which these assemblies are updated during an odour response. Neural coding with oscillations thus allows combinatorial representations in time as well as in space.

Although stimulus-evoked oscillations of brain potentials caused by synchronized neural activity have been known for about 50 years, the roles, if any, they might play in information coding remain conjectural. We tested two functional hypotheses of temporal codes that use oscillations. The first proposes that oscillations, by virtue of their periodic nature, allow the phase of neural signals (that is, the timing of action potentials relative to a specific or common reference during each cycle) to be a coding parameter. Different and possibly coexisting stimuli could thus be represented by different neural assemblies, respectively defined by a common phase of activity[10,11,13,16,17]. This hypothesis predicts that the neural assemblies activated by different stimuli should synchronize at different phases. The second hypothesis rather proposes that oscillations allow the rank order (for example, cycles 1, 2 and 4 of the oscillation) of action potentials produced by participating neurons to be coding parameters. In this scheme the order of recruitment of neurons in an oscillating assembly should be stimulus-specific.

To test these hypotheses, we used the olfactory antennal lobe of the locust, in which individual odours are represented combinatorially by oscillating and dynamic neural assemblies, each formed by about 10% of a total of about 800 projection neurons (PNs)[8,14,15]. We recorded simultaneously the responses of small ensembles (2–5) of PNs—the analogues of the mitral-tufted cells of the vertebrate olfactory bulb—*in vivo*, to airborne odourants. Figure 1*a* illustrates the temporally modulated responses of two PNs to a cherry blend. Although both neurons responded in part

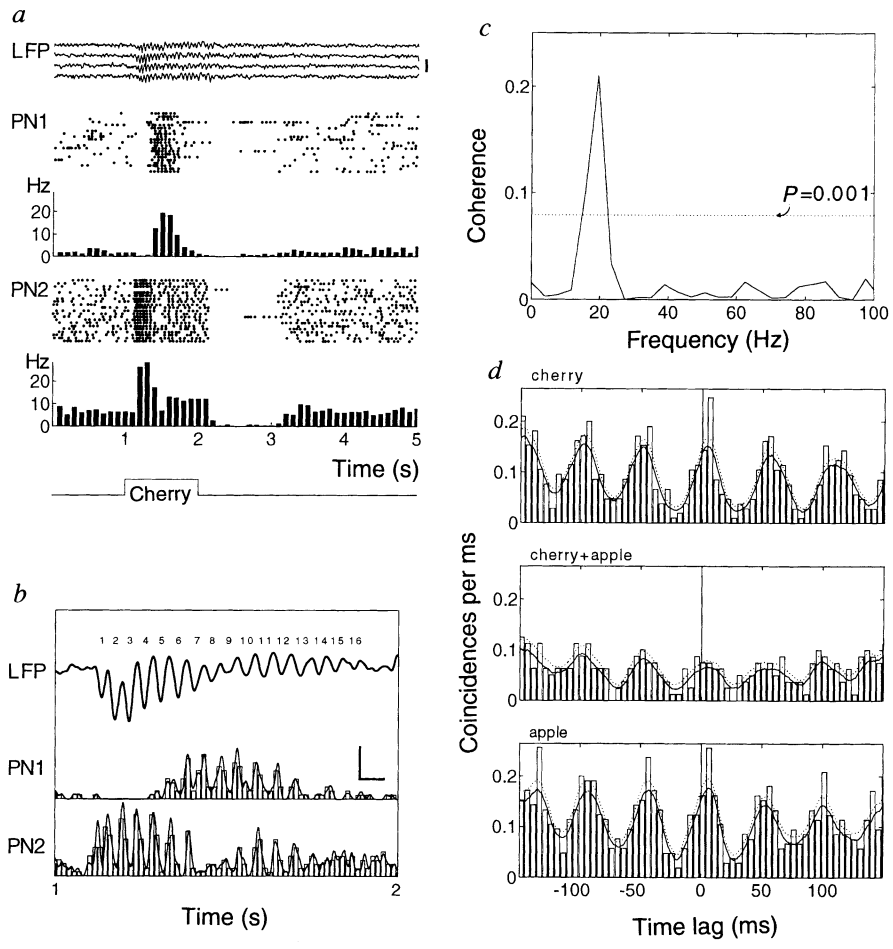

FIG. 1 Odours evoke reliable temporal response patterns in projection neurons, with tight oscillatory synchronization and neuron-specific modulation of periodic firing probability. The phase of firing contains no information. *a*, Rasters and peristimulus histograms (PSTHs) of the responses of two simultaneously recorded antennal lobe PNs to the odour cherry (21 trials at 0.1 Hz, traces aligned on the odour delivery pulse onset). The local field potentials (LFP) recorded in the ipsilateral mushroom body during trials 1–4 are shown. Note that PN1 was briefly inhibited, later excited, and finally inhibited again, whereas PN2 was excited in two successive phases and then inhibited at the offset of the stimulus. Note the duration of the 20 Hz LFP oscillations. Calibration (LFP): 500 μV. *b*, Fine temporal structure of the PNs' responses during the 1–2 s epoch in *a*. Spikes produced by each PN over the 21 trials were binned in 15-ms bins (histograms) or convolved with a 5-ms-wide gaussian function (solid lines), giving a smooth evolution of the PN firing probability, free of binning artefacts[29]. LFP trace is average of 21, indicating very tight stimulus-locking with this odour. Note that, when both PNs fired together, their action potentions were synchronous and locked to the LFP oscillations. Calibrations: horizontal, 50 ms; vertical, 30 Hz, or $P = 0.03$ of firing per 1 ms bin. Probability of firing during any period is obtained by integrating the solid line over this period, provided that it does not exceed the shortest interspike interval (which might result in $P > 1$). *c*, Coherence function[18] (varies between 0 and 1) calculated for the spikes produced by these two PNs over the 1-s-long epoch in *b* over all 21 trials. The peak at 20 Hz well exceeds the $P = 0.001$ significance level. *d*, Crosscorrelation functions calculated between the spike trains produced by both PNs in *a* and *b*. Spike coincidences summed, respectively, over 21, 16 and 21 trials for cherry, cherry + apple and apple, were binned in 5-ms bins (histograms) or convolved with a 5-ms-wide gaussian function (solid lines). Dotted lines indicate one standard deviation of the mean. Note that the roughly 5 ms delay between the two PNs (PN1 leading) is independent of the odour.

TABLE 1 Firing probabilities of neurons in response to odours

Cherry + apple

Prior probabilities

		Cycle 1	Cycle 2	Cycle 3
	P(PN1)	**0.96**	0.87	0.39
	P(PN2)	0.04	0.70	0.52

Joint probabilities: *P*(PN1,PN2)

		PN1 Cycle 1	PN1 Cycle 2	PN1 Cycle 3
PN2	Cycle 1	0.04	0.04	0
	Cycle 2	0.65	0.61	0.26
	Cycle 3	0.48	0.43	0.22

Conditional probabilities: *P*(PN1 | PN2)

		PN1 Cycle 1	PN1 Cycle 2	PN1 Cycle 3
PN2	Cycle 1	1.0	1.0	0
	Cycle 2	0.94	0.88	0.38
	Cycle 3	0.92	0.83	0.42

Conditional probabilities: *P*(PN2 | PN1)

		PN1 Cycle 1	PN1 Cycle 2	PN1 Cycle 3
PN2	Cycle 1	0.05	0.05	0
	Cycle 2	0.68	0.70	0.67
	Cycle 3	0.50	0.50	0.56

Geraniol + cherry

Prior probabilities

		Cycle 1	Cycle 2	Cycle 3	Cycle 4
	P(PN1)	**0.60**	0.50	0	0
	P(PN2)	0	0	**0.40**	0.30

Joint probabilities: *P*(PN1,PN2)

		PN1 Cycle 1	PN1 Cycle 2	PN1 Cycle 3	PN1 Cycle 4
PN2	Cycle 1	0	0	0	0
	Cycle 2	0	0	0	0
	Cycle 3	0.40	0.30	0	0
	Cycle 4	0.20	0.20	0	0

Conditional probabilities: *P*(PN1 | PN2)

		PN1 Cycle 1	PN1 Cycle 2	PN1 Cycle 3	PN1 Cycle 4
PN2	Cycle 1	–	–	–	–
	Cycle 2	–	–	–	–
	Cycle 3	**1.0**	0.75	0	0
	Cycle 4	0.67	0.67	0	0

Conditional probabilities: *P*(PN2 | PN1)

		PN1 Cycle 1	PN1 Cycle 2	PN1 Cycle 3	PN1 Cycle 4
PN2	Cycle 1	0	0	–	–
	Cycle 2	0	0	–	–
	Cycle 3	**0.67**	0.60	–	–
	Cycle 4	0.33	0.40	–	–

Action potentials of one PN during a given oscillation cycle have predictive value about the likelihood of firing of another PN during the same or a different cycle. Firing probabilities of the two PNs in Figs 2 and 3 during the first few cycles are shown for cherry + apple (left) and geraniol + cherry (right). The 'prior' probability is the probability that a PN fired an action potential in a given cycle. The 'joint' probability (*P*(PN*x*, PN*y*)) is the probability that PNs *x* and *y* fired together during the same trial, with a specific temporal relationship (for example, PN1 in cycle 1 and PN2 in cycle 3). The 'conditional' probability (*P*(PN*y* | PN*x*)) is the probability that PN*y* fired an action potential during a given cycle, given that PN*x* fired an action potential in the same, or a different cycle, of the same trial (for example, the conditional probability that PN2 fired an action potential in cycle 3, given that PN1 had fired in cycle 1 of the same trial, was 0.67 in response to geraniol + cherry). See text for details; numbers in bold are referred to in the text. When conditional probabilities so calculated were greater than the corresponding prior probabilities, they exceeded them by an amount varying between 0 and 0.45. The average increase was 0.21 ± 0.085 ($n = 45$).

with an increased firing rate, their peaks of activity did not coincide and the durations of the periods of increased firing differed between them. Figure 1*b* illustrates the fine temporal structure of these responses, revealing that the firing probability of each PN varied rhythmically and that the timing of either neuron's activity was locked to the other's and to the field potential oscillation. The magnitude squared coherence[18] of the activity of these two PNs over the 1-s response period was significantly different from zero ($P < 0.001$) at 20 Hz, the frequency of the field potential oscillations (Fig. 1*c*), indicating tightly correlated firing. We presented 13 odours and their mixtures. For all odours with which the recorded neurons phase-locked to the field potential, we measured the phase of each neuron relative to the field potential (not shown) or to the other neuron (Fig. 1*d*), by cross-correlating their responses. Figure 1*d*, for example, indicates that, although these two neurons fired and phase-locked in response to cherry, apple, or a mixture of both, the slight phase difference between their action potentials was constant and thus not odour specific. This analysis was repeated with five pairs of PNs and 17 'neuron pair-odour' combinations for which coherence values were significant at $P < 0.01$. In no case did the phase of action potentials relative to the field potential or to action potentials of other participating neurons appear to vary with, and thus participate in encoding, the stimulus.

We next considered the second hypothesis. Figure 1*b*, for example, indicates that, although both neurons were synchronized in response to cherry, coincident firing of both PNs occurred only during certain cycles of the oscillatory ensemble response (for example, cycles 6–7, 10–13), and never during other cycles (for example, 1–4). This information cannot be extracted by cross-correlation analysis (Fig. 1*d*), which averages together successive events, thereby obscuring the temporal details of correlated activity. Are such temporal patterns reliable and stimulus-specific? Figure 2*Aa*, *Ba* illustrates the gross responses of a different pair of neurons to the odour apple and the mixture cherry + apple. In both cases, the two neurons produced remarkably similar responses: a short 'burst' of action potentials, a period of silence and a second, longer period of elevated activity. These responses (rasters and peristimulus histograms) seemed, at first glance, to be identical for both odours. Consider now their fine temporal structure during the first 500 ms of the response (Fig. 2*Ab*, *Bb*). Whereas PNs 1 and 2 both fired reliably during cycles 1–3 in response to apple (Fig. 2*Ab*), PN2 failed to fire during cycle 1 in response to the mixture, resulting in a relative shift of the two PNs' firing by one cycle (Fig. 2*Bb*). Such 1- or 2-cycle relative shifts were observed for several other odour combinations to which both neurons responded (Fig. 3). The skewness of the crosscorrelation functions calculated over two PNs' responses to odours could be indicative of the absence (for example, Fig. 2*Ac*) or presence (for example, Fig. 2*Bc*) of a sequential activation of the two neurons, but could not reveal the exact temporal structure of these sequences.

These fine temporal patterns were highly reliable. First, the firing probability of a PN during a given cycle could exceed 0.9 (for example, cycle 1 for PN1 in response to cherry + apple; Fig. 3 and Table 1), indicating participation of this PN in the odour-coding assembly during this cycle of almost any trial. Second, the firing of one PN during a given cycle often had some predictive value about

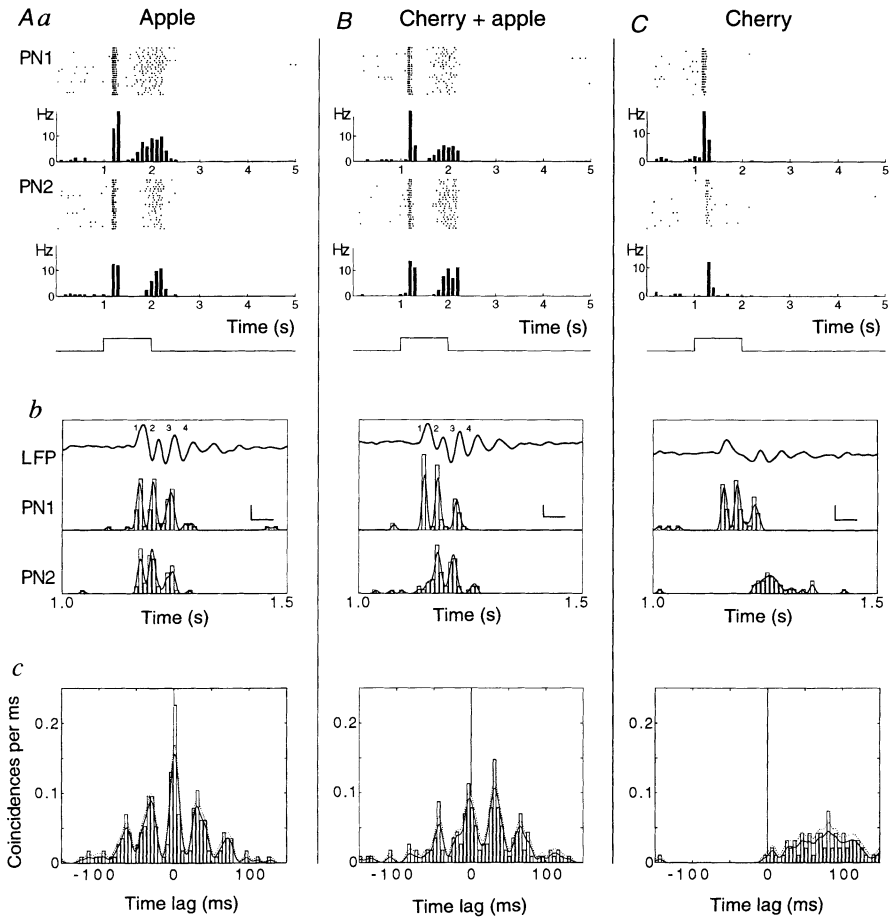

FIG. 2 Stimulus identity is encoded in part by the fine temporal features of firing of groups of neurons. *A–C*, Responses of two PNs (different animal to that in Fig. 1) to two odours (*A*, *C*) and their 1:1 mixture (*B*). *a*, Rasters and PSTHs constructed as in Fig. 1*a*. *b*, Fine temporal structure of the PNs' responses during the 1–1.5 s epoch (representation as in Fig. 1*b*, bin size: 10 ms). *c*, Crosscorrelation functions calculated with the PNs spike trains (as in Fig. 1*d*). Note the similarity of both neurons' overall responses to apple and cherry + apple (*Aa*, *Ba*), but the striking difference between the fine structures of their spike trains (*Ab*, *Bb*). Note that the cross-correlation function is symmetrical about the *y*-axis at $x = 0$ (zero time lag) for apple (indicating near perfect average synchrony), but that it is skewed to the right (meaning that PN1 fired one cycle earlier on average than PN2) for cherry + apple. The exact temporal sequence of activation, however, can only be seen in *b*. Note, finally, that the response to cherry alone was shorter in both neurons (it lacked the second excitatory epoch, *Ca*), and that only PN1 showed an oscillatory response to this odour (*Cb*, *c*). Calibrations (*b*): horizontal, 50 ms; vertical, 20 Hz, or $P = 0.02$ of firing per 1 ms bin.

the behaviour of another PN during the same, or a different, cycle. For example, although the firing probability of PN2 at cycle 3 was 0.4 in response to geraniol + cherry, this probability rose to 0.67 if it was known that PN1 had fired at cycle 1 (Table 1). Similarly, whereas the firing probability of PN1 at cycle 1 was 0.6 in response to this odour, it rose to 1.0 if it was known that PN2 would also fire at cycle 3 (Table 1). These results show that odours can reliably evoke specific sequences of activity across neural assemblies.

The fine temporal structure of PN responses to mixtures were not simple or predictable combinations of their responses to the components presented separately (compare Fig. 2*A–C*). Each odour, however complex, apparently evoked activity in its own specific neuronal set and its own specific sequence of activity (coarse and fine levels of analysis, Fig. 2). For example, unique patterns are discernible in the firing probabilities of the two PNs in Fig. 2 in response to many other odours (Fig. 3). Each oscillation cycle is represented by a different colour, and the existence of a firing probability greater than 0.3 for each PN and cycle is indicated by a coloured box. This representation reveals six different patterns for these nine odours (Fig. 3), indicating that knowing the average temporal firing behaviour of these two neurons over four oscillation cycles provides a 0.66 chance of correct odour identification. Ignoring this temporal information would, by contrast, provide only a 0.33 chance of correct identification (three different spike counts for nine odours), a probability similar to that provided by considering the temporal firing behaviour of one only of these two PNs (3 different temporal patterns for 9 odours in each PN; Fig. 3). In reality, PN firing is probabilistic and average firing probabilities are not available to the animal on a single odour sampling. Information is, therefore, probably gathered from multiple neurons at once as well as over several oscillation cycles. Previous results indicate that odours are probably represented by about 100 neurons[8,15]; only a subgroup of these are likely to be coactive during any given oscillation cycle.

In summary, we have shown that odours evoke activity in neural assemblies that are updated non-randomly at each cycle of an oscillatory response pattern. Information about the stimulus is found not in the phase of the active neurons (which is statistically invariant when neurons synchronize to each other) but rather in their identity[8,14,19,20] and in the temporal pattern in which they are recruited (this study). The firing probability of individual neurons during one cycle of the response can be linked to that of other neurons during the same or other cycles, indicating deterministic and stimulus-specific sequential activation of groups of neurons. In principle, the timing of these odour-encoding sequences need not be precisely locked to the stimulus, although it is this feature which allowed us to detect them. We propose that oscillations are a means to encode stimuli in a temporal combinatorial fashion. In this hypothesis, stimuli are represented both by spatial (instantaneous) ensembles, that is, the neurons activated together during any given cycle, and by temporal sequences, reflected in the responses of individual or groups of neurons over several cycles. Given the probabilistic nature of any neuron firing in any one cycle of the oscillatory response, the information provided by spatial ensembles alone is often ambiguous. We propose that the brain reduces the ambiguity by assigning 'meaning' to the pattern in which these ensembles succeed each other. In particular, such a mechanism might aid reliable and rapid stimulus identification. In mammals, for example, each inspiration evokes 5–10 cycles of gamma frequency (30–60 Hz) oscillations in the olfactory bulb[21,22]. In insects, behavioural studies indicate that odour identification is possible in a few hundred milliseconds[23], allowing in principle only 4–6 cycles of 20–30 Hz oscillations[15]. Such a coding mechanism might also occur in any sensory system (cortical or not) expressing

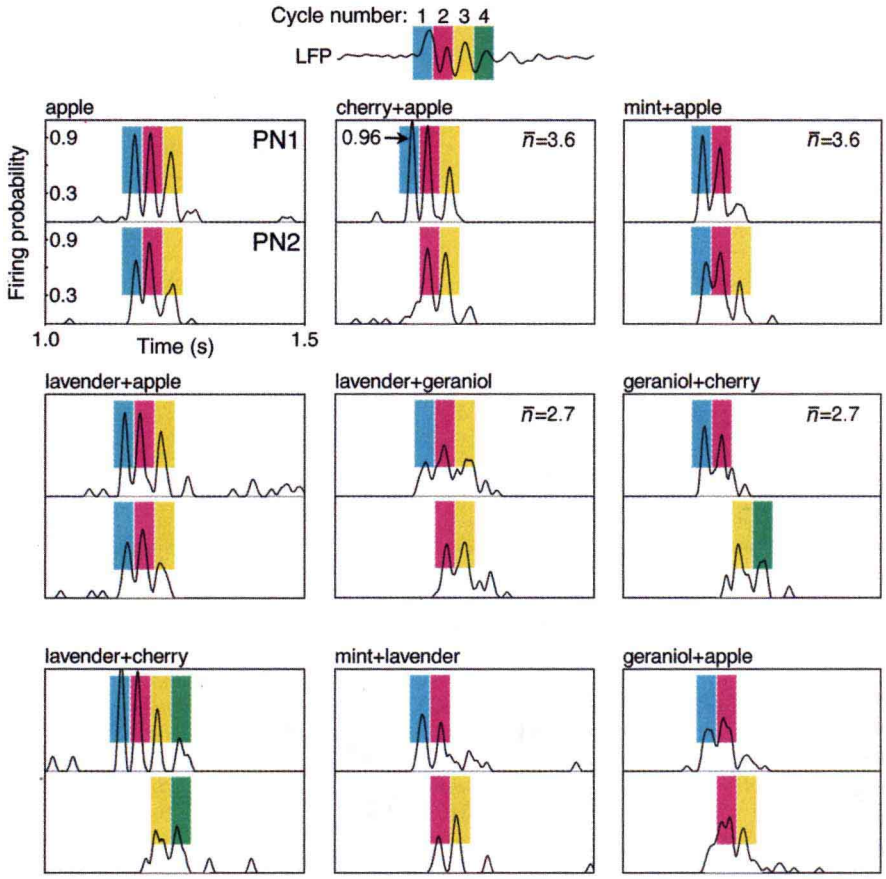

FIG. 3 Information about an odour can be gained from the temporal structure of firing of the neurons activated in periodic synchrony. The temporal evolution of the firing probabilities of the two PNs in Fig. 2 in response to nine complex odours is displayed here. If the firing probability of either PN exceeded a given threshold ($P = 0.3$) during one oscillation cycle of the response, the neuron's action potential was assigned a colour corresponding to the cycle in which it occurred. A coloured box thus indicates that the corresponding PN fired an action potential during that cycle with a probability $P > 0.3$ (integrated over the 20 ms period centred on the peak firing probability). The average LFP in response to apple is shown at the top, with each oscillation cycle denoted by its colour. Each odour can thus be represented by a particular coloured pattern that contains more information about odour identity than spike count alone. For example, whereas cherry + apple and mint + apple each produced an average of 3.6 action potentials per trial in the two PNs over the first 3 cycles, the two odours could be discriminated because these action potentials occurred in a different order with each odour. Similarly, lavender + geraniol and geraniol + cherry each produced an average of 2.7 action potentials per trial in the two PNs over the first four cycles, but the two odours could be discriminated by the sequence of these action potentials.

oscillatory synchronization, such as the visual[3,17] and somatosensory[24] cortices of mammals. Evidence from flies and from rat, cat and primate neocortical neurons *in vitro*[25] and *in vivo*[26,27,28] is also consistent with the possibility that spike timing might play a role in information coding there, although these studies did not consider spike timing within the context of oscillatory synchronization. This study shows that oscillations can support combinatorial coding in time, and that information about a stimulus is contained in the precise temporal firing pattern of groups of neurons. □

Methods

Forty adult locusts (*Schistocerca americana*) of both sexes taken from a crowded colony were immobilized with one antenna intact, as in ref. 14. A window was cut open on the head and the brain was gently desheathed and intermittently superfused with locust saline (in mM: 140 NaCl, 5 KCl, 5 $CaCl_2$, 4 $NaHCO_3$, 1 $MgCl_2$, 6.3 HEPES, pH 7.0).

Odour stimulation. Airborne odour puffs (1 s long, 0.3 l min^{-1}) were delivered from a circular array of stainless steel nozzles placed 21 mm in front of the antenna. All nozzles were angled so as to converge on the antenna. Clean, dry air was constantly delivered at a rate of 0.3 l min^{-1}. Each odour (10 µl of apple, vanilla, strawberry (Gilberties, Easton, CT), cherry (Bell Flavors and Fragrances Inc.), spearmint (Flavco, Mansfield, OH), lavender (Nuit Unlimited), eugenol, geraniol (Sigma), cineole, isoamylacetate, citral (Aldrich), crushed banana, alfalfa chow) was carried by a distinct nozzle to exclude crosscontamination along the odour path. Mixtures were applied by simultaneously delivering selected pairs of odours, each at the rate of 0.3 l min^{-1}.

Electrophysiology. Each PN (up to five simultaneous recordings) and the local field potential (LFP) were recorded extracellularly with blunt glass micropipettes (horizontal puller; Sutter, Novato, CA) filled with saline, and amplified with DC amplifiers (Axon, Foster City, CA; NPI, Adams-List). Traces were stored on digital tape (Micro Data Inc., 5.5 kHz cut-off) and analysed off-line, using National Instruments NBMI16L hardware and LabVIEW (National Instruments) and MatLab (The MathWorks) software. PN action potential times were obtained by applying a digital threshold discriminator algorithm to traces containing a singular action potential waveform. PN isolation was thus unambiguous. LFP traces were low pass filtered at 50 Hz (digital non-causal 5-pole Butterworth). The data presented come from 200 neuron pairs. Of these, 45 pair-odour combinations showed sufficiently long epochs of coincident firing of the two neurons. These were analysed exhaustively, providing 17 (from 5 different neuron pairs) with a coherence[18] at 20–30 Hz that was statistically significant at $P < 0.01$. Given that individual odours probably evoke synchronized activity in about 10% of the 830 PNs[8], the chance of recording simultaneously from 2 neurons that synchronize in response to the same odour should be about 1% of the obtained pairs. Our results are in good agreement with these estimates.

Statistics. Prior and joint probabilities were computed by counting the mean number of action potentials (prior) or coincidences (joint) in 10 ms epochs centred on the peaks of the firing probability curve in each cycle (peaks of solid lines in Figs 2*b* and 3). Conditional probabilities are the quotient of the joint and prior probabilities. Because the PNs never fired more than once during any cycle, normalization was not necessary and these values varied between 0 and 1. Because conditional probabilities are ratios, they are undefined (denoted by a dash in Table 1) when the prior probability in the denominator is zero.

Received 8 July; accepted 20 September 1996.

1. Adrian, E. D. *J. Physiol. (Lond.)* **100,** 459–473 (1942).
2. Freeman, W. J. *J. Neurophysiol.* **23,** 111–131 (1960).
3. Gray, C. M. & Singer, W. *Proc. Natl Acad. Sci. USA* **86,** 1698–1702 (1989).
4. Hubel, D. H. & Wiesel, T. N. *J. Neurophysiol.* **28,** 229–289 (1965).
5. Pöppel, E. & Logothetis, N. *Naturwissenschaften* **73,** 267–268 (1986).
6. Gelperin, A. & Tank, D. W. *Nature* **345,** 437–440 (1990).
7. Laurent, G. & Naraghi, M. *J. Neurosci.* **14,** 2993–3004 (1994).
8. Laurent, G. & Davidowitz, H. *Science* **265,** 1872–1875 (1994).
9. Gray, C. M. *J. Comput. Neurosci.* **1,** 11–38 (1994).
10. Singer, W. *Concepts Neurosci.* **1,** 1–26 (1990).
11. Hopfield, J. J. *Nature* **376,** 33–36 (1995).
12. Milner, P. *Psychol. Rev.* **81,** 521–535 (1974).
13. von der Malsburg, C. *The Correlation Theory of Brain Function* 81–82 (Internal Report, MPI für Biophysikalische Chemie, Göttingen, Germany, 1981).
14. Laurent, G., Wehr, M. & Davidowitz, H. *J. Neurosci.* **16,** 3837–3847 (1996).
15. Laurent, G. *Trends Neurosci.* (in the press).
16. von der Malsburg, C. & Schneider, W. *Biol Cybern.* **54,** 29–40 (1986).
17. Singer, W. & Gray, C. M. *Annu. Rev. Neurosci.* **18,** 555–586 (1995).
18. Brillinger, D. *Time Series* (Holden-Day, San Francisco, 1981).
19. Shepherd, G. M. *Neuron* **13,** 771–790 (1994).
20. Cinelli, A. R., Hamilton, K. A. & Kauer, J. S. *J. Neurophysiol.* **73,** 2053–2071 (1995).
21. Gray, C. M. & Skinner, J. E. *Exp. Brain Res.* **69,** 378–386 (1988).
22. Bressler, S. L. & Freeman, W. J. *Electroencephalogr. Clin. Neurophysiol.* **50,** 19–24 (1980).
23. Smith, B. H. & Menzel, R. *Ethology* **82,** 68–81 (1989).
24. Murthy, V. N. & Fetz, E. E. *Proc. Natl Acad. Sci. USA* **89,** 5670–5674 (1992).
25. Mainen, Z. F. & Sejnowski, T. J. *Science* **268,** 1503–1506 (1995).
26. Abeles, M., Bergman, H., Margalit, E. & Vaadia, E. *J. Neurophysiol.* **70,** 1629–1638 (1993).

27. Middlebrooks, J. C., Clock, A. E., Xu, L. & Green, D. M. *Science* **264,** 842–844 (1994).
28. Bialek, W., de Ruyter van Steveninck, R. & Warland, D. *Science* **252,** 1854–1857 (1991).
29. Paulin, M. G. *Biol. Cybern.* **66,** 525–531 (1992).

ACKNOWLEDGEMENTS. We thank E. M. Schuman, F. Gabbiani and members of the Laurent laboratory for their comments on the manuscript. Supported in part by an Office of Naval Research graduate student fellowship to M.W. and an NSF grant and NSF Presidential Faculty Fellow award to G. L.

CORRESPONDENCE and requests for materials should be addressed to G. L. (e-mail: laurentg@starbase1.caltech.edu).

Spatio-temporal dynamics of cyclic AMP signals in an intact neural circuit

Chris M. Hempel*, Pierre Vincent†, Stephen R. Adams†, Roger Y. Tsien†‡ & Allen I. Selverston*

Departments of * Biology and † Pharmacology and ‡ Howard Hughes Medical Institute, University of California, San Diego, La Jolla, California 92093, USA

The functional properties of neuronal networks can be reconfigured by a variety of modulatory neurotransmitters, which may alter the excitable properties of neurons or the strengths of synaptic connections. Many of these neuromodulators act via the intracellular second messenger cyclic AMP, but their effects on the spatial distribution of cAMP concentration have never been examined in an intact neural circuit. We therefore used the cAMP-indicator dye FICRhR (refs 1, 2) to investigate the effect of several neuromodulators (octopamine, dopamine, acetylcholine, serotonin and proctolin) on cAMP distribution in identified neurons of the lobster stomatogastric ganglion (STG). When added to the bath solution, each of these neuromodulators produced a unique pattern of cAMP transients among the different neurons of the STG. Electrical stimulation of neurons innervating the STG causes synaptic release of endogenous modulators, leading within a few seconds to local increases of cAMP in fine neurite branches, the site where many modulators are thought to act[3,4]. After prolonged stimulation, cAMP diffuses from the site of production to throughout the neuritic tree and eventually to the cell body. Diffusion of cAMP may explain how transient localized inputs to a neuron can produce long-range effects such as long-term changes in gene expression.

The stomatogastric ganglion of the spiny lobster *Panulirus interruptus* comprises about 24 interconnected motor neurons and 6 interneurons arranged into two central pattern generators that control the striated muscles of the stomach[5]. The neural circuitry of the STG can be reconfigured by any of the approximately twenty neuromodulators that are known to be released onto the ganglion by afferent fibres in the stomatogastric nerve (STN)[6]. The actions of at least some of these modulators are believed to be mediated by cAMP[7]. We have used cAMP imaging in the STG to examine the signal transduction events that underlie circuit reconfiguration.

The stomatogastric nervous system was removed from adult lobsters using a standard dissection procedure[8] that leaves the neural circuitry of the STG and its modulatory inputs intact. After electrophysiological identification, STG neurons were pressure-injected with fluorescein- and rhodamine-labelled cAMP-dependent protein kinase (PKA) type II (FlCRhR; refs 1, 2) to image cAMP concentration ([cAMP]) by high-speed confocal microscopy[9] (Fig. 1*a*). The ratio of fluorescein to rhodamine emissions from FlCRhR is sensitive to cAMP concentrations over the range 0.05–10 μM at the ionic strength of marine invertebrate cytoplasm[10]. Unfortunately in this preparation it was difficult to use cAMP antagonists to impose an effectively zero cAMP concentration [cAMP] in order to determine the minimum fluorescence ratio and so calibrate FlCRhR signals in terms of absolute [cAMP]. Therefore, our main conclusions rely only on relative changes in [cAMP] over time. Application of the adenylyl cyclase activator forskolin to the STG increased the ratio to a level that could not be raised further by the phosphodiesterase inhibitor IBMX and the membrane-permeable PKA activator S_p-5,6-Cl_2-cBIMPS, showing that forskolin increased [cAMP] enough to saturate the FlCRhR ratio change. All the responses to neuromodulators described showed a ratio change smaller than the saturating forskolin response, that is, less than 10 μM free cAMP.

Bath application of several modulators known to be present in STN fibres produced transient increases of somatic [cAMP]. These transients were cell-specific, that is, each modulator produced a distinct pattern of responses across the ganglion (Fig. 1*b–d*; Table 1). The patterns of [cAMP] transients were accompanied by well known changes in the electrophysiological output of the circuit[11–14], which did not seem to be affected by FlCRhR or by imaging (Fig. 2). As cAMP has powerful effects on the electrophysiological activity of STG neurons[7], the observed pattern of cAMP responses must contribute substantially to the electrophysiological changes. However, comparisons of the patterns of [cAMP] changes with the cell-specific patterns of electrophysiological effects of each modulator did not show any simple correspondence between the two, indicating that the relationship is complex, and probably involves other second messenger pathways.

To determine the effect of synaptic release of endogenous neuromodulators on [cAMP] in postsynaptic cells, we directly stimulated neuromodulatory afferent fibres in the STN. Extracellular STN stimulation lasting 2–3 min elicited [cAMP] transients in the somata of many STG neurons (Fig. 2*a*, *b*). However, the latencies of somatic [cAMP] transients induced by STN stimulation were far too long to account for the rapid electrophysiological effects that occur within seconds of STN stimulation[15,16]. This suggested that responses would be faster in other regions of the cell. STG neurons are complex structures with an extensive neuritic arbor which could be imaged in cells well filled with FlCRhR (Fig. 3*a*). The fastest [cAMP] increases were seen in the finest neurites (2–3 μm diameter) that we were able to image (for example, see Fig. 3*c*). As little as one second of STN stimulation was sufficient to produce a detectable [cAMP] increase in these fine neurites. Larger neurites did not respond at all to such short stimuli. Response latencies were as low as 3 s, with a mean of 6.6 s for the most rapidly responding neurites in five separate neurite fields from three preparations. We expect that the response kinetics of the finest neurites in the ganglion (less than 1 μm diameter), which were below our threshold for detection, would be fast enough to account for the electrophysiological changes that can be brought about in just a few seconds by STN stimulation[16]. The location of the rapid transients is also appropriate, because the synaptic structures[3], and probably some of the ionic conductances[4] that are the targets of neuromodulation, are located preferentially on neuritic branches of these neurons.

Imaging neurites during longer periods of STN stimulation revealed a centripetal pattern of [cAMP] increases, with finer neurites responding most rapidly (24 ± 4 s to 50% of maximum response; $n = 20$, mean ± s.e.m.), then primary neurites (53 ± 6 s; $n = 20$) and finally somata (245 ± 35 s; $n = 15$) (Fig. 3*b*, *c*). The difference in response times between higher-order neurites and primary neurites and between primary neurites and somata were both statistically significant (Student's *t*-test, $P < 0.01$).

As cAMP is produced at the membrane by adenylyl cyclase and subsequently diffuses into the cytosol, the faster [cAMP] elevations in smaller neurites could be solely a result of their larger surface-area-to-volume ratio[17]. Three observations are inconsistent with this hypothesis. First, STN-induced [cAMP] elevations in larger neurites and somata were delayed relative to finer neurites